JOC The Journal of Organic Chemistry

Article

pubs.acs.org/joc

Mechanism and Enantioselectivity of Dirhodium-Catalyzed Intramolecular C−H Amination of Sulfamate

Xiting Zhang,[†,‡] Zhuofeng Ke,[†] Nathan J. DeYonker,[§] Huiying Xu,[†] Zhi-Feng Li,[†] Xianyan Xu,[†] Xuepeng Zhang,[†] Cheng-Yong Su,*[,†] David Lee Phillips,[‡] and Cunyuan Zhao*[,†]

[†]MOE Key Laboratory of Bioinorganic and Synthetic Chemistry/KLGHEI of Environment and Energy Chemistry, School of Chemistry and Chemical Engineering, Sun Yat-Sen University, Guangzhou 510275, P. R. China

[‡]Department of Chemistry, The University of Hong Kong, Pokfulam Road, Hong Kong, P. R. China

[§]Department of Chemistry, The University of Memphis, Memphis, Tennessee 38152, United States

Supporting Information

ABSTRACT: The mechanisms and enantioselectivities of the dirhodium (Rh_2L_4, L = formate, *N*-methylformamide, *S*-nap)-catalyzed intramolecular C−H aminations of 3-phenylpropylsulfamate ester have been investigated in detail with BPW91 density functional theory computations. The reactions catalyzed by the $Rh_2^{II,II}$ catalysts start from the oxidation of the $Rh_2^{II,II}$ dimer to a triplet mixed-valent $Rh_2^{II,III}$−nitrene radical, which should facilitate radical H-atom abstraction. However, in the Rh_2(formate)$_4$-promoted reaction, as a result of a minimum-energy crossing point (MECP) between the singlet and triplet profiles, a direct C−H bond insertion is postulated. The Rh_2(*N*-methylformamide)$_4$ reaction exhibits quite different mechanistic characteristics, taking place via a two-step process involving (i) intramolecular H-abstraction on the triplet profile to generate a diradical intermediate and (ii) C−N formation by intersystem crossing from the triplet state to the open-shell singlet state. The stepwise mechanism was found to hold also in the reaction of 3-phenylpropylsulfamate ester catalyzed by Rh_2(*S*-nap)$_4$. Furthermore, the diradical intermediate also constitutes the starting point for competition steps involving enantioselectivity, which is determined by the C−N formation open-shell singlet transition state. This mechanistic proposal is supported by the calculated enantiomeric excess (94.2% *ee*) with the absolute stereochemistry of the product as *R*, in good agreement with the experimental results (92.0% *ee*).

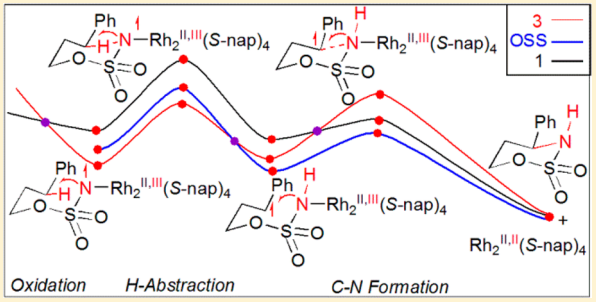

INTRODUCTION

A saturated C−H bond-activation/C−N bond-forming reaction catalyzed by a transition-metal catalyst has been the subject of many studies and considered among standard synthetic protocols in recent years.[1] Among them, the intramolecular C−H amination of sulfamate and carbamate esters that relies on dirhodium complexes (Rh_2L_4) as the catalyst has been widely utilized with a high degree of chemo- and regioselectivity,[2] although other metals can also be used for this purpose, particularly ruthenium porphyrins.[3]

It has been generally assumed that metal-mediated intramolecular aminations involve the following steps: in situ generation of an iminophenyliodinane from the substrate, formation of the Rh_2−nitrene active intermediate, and C−H activation/C−N bond formation,[4] with the last step considered to be product-determining. Previous experimental and theoretical studies have anticipated two mechanistic proposals for C−H activation/C−N formation, namely, the concerted and stepwise (or radical) mechanisms (Figure 1). The concerted pathway starting from the closed-shell singlet state of the metal (Cu,[4c] Rh_2,[4a,5] or Ru[6])−nitrene goes through a hydride transfer/C−N formation transition state (TS). An alternative pathway beginning with an open-shell electronic state (doublet, triplet, etc.) of the metal (Co, Rh_2, Fe, or Ru_2)−nitrene is a stepwise mechanism. The first step via a H-abstraction transition state gives rise to a radical intermediate. The second step involves C−N bond formation, which may be a barrier-free process according to some theoretical reports[4a,c,5−7] (stepwise pathway I) but involves an identifiable transition state in other papers (stepwise pathway II).[8] Cundari

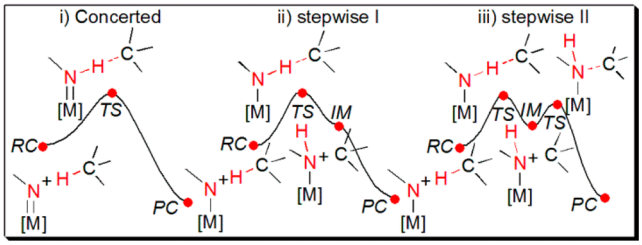

Figure 1. Three mechanistic pictures of the C−H activation/C−N bond formation catalyzed by metal−nitrene complexes.

Received: September 28, 2013
Published: November 26, 2013

and co-workers[3c,9] suggested that the open-shell singlet is the ground state for some Cu-centered complexes.

Rhodium-centered complexes are high-quality catalysts for intramolecular C−H aminations. However, it is clear that the mechanism is still under debate. When sulfamates and carbamates are used as nitrene precursors, it is generally accepted that the reaction takes place via a concerted asynchronous insertion of a singlet Rh_2−nitrene, particularly in the case of highly reactive substrates.[2a,c,d,f,h−k,4b,10] This scenario is supported by density functional theory (DFT) studies,[4a,5] experimental studies of the Hammett relationship, the kinetic isotope effect (KIE), the absence of ring-opened products using a cyclopropyl radical clock, and the stereospecific nitrene insertion with retention of configuration.[4b,11] However, an extremely fast recombination of radical species (estimated lifetime: 200 fs) cannot be ruled out.[1b,2h] Dauban and co-workers cast some doubt that these physical organic experiments could be used for unambiguous elucidation of the reaction pathway of C−H amination.[12] Both computational and experimental data recently suggested a stepwise mechanism for a diruthenium-mediated C−H insertion, but still no ring-opening products could be detected.[7a] A KIE of 6.7 in the dirhodium-promoted intramolecular amination was observed by Driver,[13] which implied a stepwise transition state. No clear-cut conclusion can therefore be drawn from KIE values except that C−H bond cleavage might be a rate-limiting step. Pérez reported that a stepwise pathway can also lead to stereospecific nitrene insertion with retention of configuration.[14] Recent studies of the dirhodium-promoted intermolecular C−H amination reaction by Du Bois suggested that a stepwise C−H abstraction/radical rebound pathway may be operative.[1a] Liu also found via theoretical calculations that the Rh_2-mediated amination reaction occurs through a stepwise pathway.[15]

In the present paper, part of our theoretical focus is on the intramolecular C−H amination of sulfamate catalyzed by Rh_2(*S*-nap)$_4$ (Figure 2), the system developed by Du Bois.[2h]

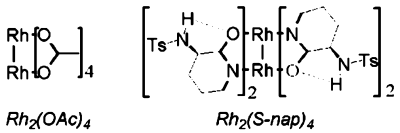

Figure 2. Two catalysts, Rh_2(OAc)$_4$ and Rh_2(*S*-nap)$_4$, involved in the present paper.

Rh_2(*S*-nap)$_4$ exhibits unprecedented performance for the enantioselectivity of intramolecular amination with benzylic and allylic C−H bonds [enantiomeric excess (*ee*) values generally >80%]. Rh_2(*S*-nap)$_4$ prefers allylic insertion rather than aziridination in the oxidation reactions of homoallyl sulfamates, which cannot be found in any other dirhodium system. No products of cyclopropane ring opening were obtained from this reaction. Du Bois pointed out that the above experimental results are somewhat contradictory in terms of unambiguously pointing toward one pathway, either concerted or stepwise. The results of a cyclopropyl radical clock experiment were consistent with a concerted nitrene-type oxidation. However, Du Bois and co-workers pointed out that stepwise pathways could not be ruled out. They thought that the bias for Rh_2(*S*-nap)$_4$ toward allylic insertion intimates a possible change in mechanism from the concerted asynchronous nitrene pathway generally accepted for reactions catalyzed by dirhodium tetracarboxylates [e.g., Rh_2(OAc)$_4$; Figure 2].[2c,16]

In order to propose a general mechanism and to analyze the enantioselectivity for the dirhodium-promoted reaction, we carried out DFT computations. We mapped intersecting reaction pathways involving the closed-shell singlet, open-shell singlet, and triplet spin profiles as well as singlet−triplet minimum-energy crossing points (MECPs). The selectivity may be determined by the transition state of C−N formation for this dirhodium-mediated reaction rather than by the H-abstraction transition state.

CHEMICAL MODELS

In the present studies, we employed Rh_2(formate)$_4$ and Rh_2(*N*-methylformamide)$_4$ as models for dirhodium tetracarboxylate and carboxamidate complexes, respectively, in the interest of computational tractability. The reactions of 3-phenylpropylsulfamate ester mediated by Rh_2(formate)$_4$ and Rh_2(*N*-methylformamide)$_4$ (denoted as reactions A and B, respectively) are described herein (Figure 3). These models were investigated to

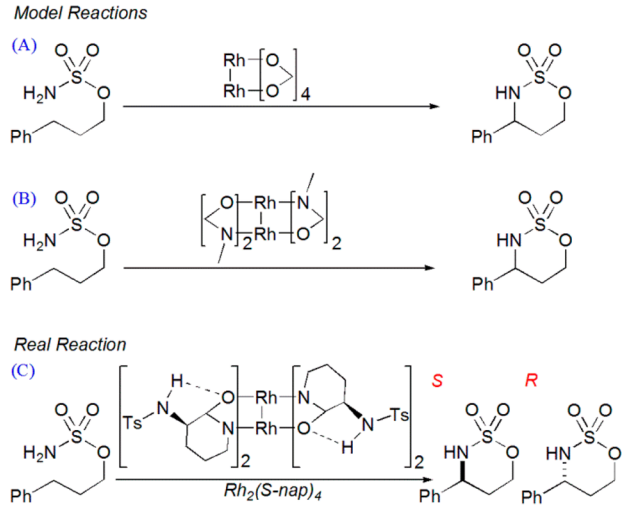

Figure 3. Three reaction systems studied in present paper: intramolecular C−H aminations of 3-phenylpropylsulfamate esters catalyzed by dirhodium tetraformate (reaction A), dirhodium tetra(*N*-methylformamide) (reaction B), and Rh_2(*S*-nap)$_4$ (reaction C).

understand the fundamental properties of the dirhodium−nitrene complexes and the mechanism of the C−H insertion reaction. The mechanism established with these models was found to hold also when studying the synthetic reaction (denoted as reaction C) (Figure 3).

In order to clearly exhibit the charge, structural changes, and spin distribution during the course of the reaction, the catalyst structure was divided into the Rh^1, Rh^2, and 4L moieties and the substrate into the R, H, and NSO_3 moieties (Figure 4).

COMPUTATIONAL DETAILS

All of the calculations were performed with the Gaussian 09 software package.[17] DFT was employed using the BPW91 pure functional,[18] which was found to validate the prediction of the singlet−triplet energy difference (E_{st}) of the dirhodium−nitrene species after comparison with the more accurate CCSD(T) method.[4a,5,15] We also investigated the effect of the functional using the BPW91, BP86, B3LYP, and TPSSh functionals (Table 1S in the Supporting Information), which again supported the BPW91 pure functional to be an economical and reliable method for the description of the E_{st} values of rhodium−nitrene species. Minimum-energy crossing points

dx.doi.org/10.1021/jo402101h | J. Org. Chem. 2013, 78, 12460−12468

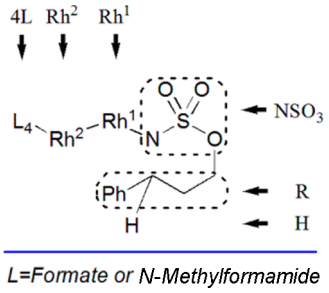

Figure 4. For clarity, 2D cartoons are divided into six moieties (Rh^1, Rh^2, 4L, R, H, and NSO_3) in reactions A and B.

(MECPs) were calculated with the MECP program of Harvey and coworkers.[19]

Geometry optimizations, harmonic vibrational frequency calculations, MECP locations, intrinsic reaction coordinate (IRC) calculations, Kohn–Sham orbital analysis, and Mulliken charge and spin-density analyses were carried out with the 6-31G* basis set for C, H, O, N, F, and S atoms and the 1997 Stuttgart relativistic small-core effective core potential (Stuttgart RSC 1997 ECP)[20] for Rh, augmented with a 4f function [ζ_f(Rh) = 1.350].[21] This composite basis set (denoted as BSI) was found to be effective for the assessment of activation free energies of Rh-centered complexes.[22] Heavy-atom basis set definitions and corresponding pseudopotential parameters were obtained from the EMSL basis set exchange library.[23] All stationary points were optimized without point-group symmetry. The stabilities of the Kohn–Sham wave functions were confirmed by stability analyses for all of the stationary points in reactions A and B at the BPW91/BS1 level.[24] Analytical second-derivative computations were performed for all stationary points in order to confirm the optimized structures as either minima or first-order saddle points. IRC[25] calculations were performed to confirm that the transition states connected the relevant reactants and products.

To evaluate the effect of solvent polarity on the energetics of the C–H amination reactions, single-point energy calculations were performed with the integral equation formalism polarizable continuum model (IEFPCM) in CH_2Cl_2 (ε = 8.93) on the gas-phase geometries. The radii and nonelectrostatic terms were taken from Truhlar and coworkers' universal solvation model (SMD).[26] Solvation single-point computations utilized a basis set (denoted as BSII) consisting of the 6-311++G** set for C, H, N, O, and S atoms and the same Stuttgart basis set as in BSI for the Rh atoms. The discussion is based on solvation Gibbs free energy (except for special annotations as indicated in the text), which was estimated as $G_{solv} = E_{solv}$(SMD-calculated) + ΔG_{corr_gas}, where E_{solv}(SMD-calculated) refers to the solvation single-point energy and ΔG_{corr_gas} refers to the thermal correction to the free energy of the solute in the gas phase.[6,7a,27]

Open-shell electronic configurations were obtained by using the broken symmetry methodology,[28] and calculated total spin density distributions of selected open-shell stationary points are summarized in Table 2S in the Supporting Information. The real energy of the open-shell singlet electronic state (E) was evaluated by considering the energy E_0 of the optimized broken-symmetry solution and the energy E_1 from separate spin-unrestricted m_s = 1 calculations at the same geometry using the formula[29]

$$E \approx \frac{S_1^2 E_0 - S_0^2 E_1}{S_1^2 - S_0^2}$$

where S_0 and S_1 are the spin contamination values of the open-shell singlet and triplet states, respectively.

RESULTS AND DISCUSSION

To understand the mechanism and enantioselectivity of the Rh_2-catalyzed amination reactions of 3-phenylpropylsulfamate ester, we performed BPW91 calculations on closed-shell singlet, open-shell singlet, and triplet pathways of reactions A, B, and C. The species involved in the reaction pathways can be listed as

Table 1. Relative Gibbs Free Energies, Electronic Energies (in Parentheses), and Solvation Gibbs Free Energies Involved in Reactions A, B, and C

species	BPW91/BSI	BPW91/BSII	species	BPW91/BSI	BPW91/BSII
^{1}**RC$_A$**	2.5 (1.9)	4.5	^{3}**MECP1$_B$**	4.0 (3.5)	5.8
^{1}**TS$_A$**	5.6 (5.2)	4.6	^{1}**MECP2$_B$**	10.5 (6.2)	9.7
PC + *Cat.*$_A$	−38.2 (−44.7)	−37.8			
^{3}**RC$_A$**	**0.0 (0.0)**	**0.0**	^{1}**RC$_C$**	7.0 (5.2)	9.5
^{3}**TS1$_A$**	7.4 (8.1)	6.8	^{1}**TS1$_C$**	24.1 (20.8)	26.0
^{3}**IM$_A$**	−3.4 (−3.7)	−5.2	^{1}**IM$_C$**	3.6 (1.8)	1.5
^{3}**TS2$_A$**	7.2 (6.1)	5.1	^{1}**TS2$_C$*R***	12.0 (6.9)	12.1
^{3}**MECP0$_A$**	4.3 (2.9)	5.6	^{1}**TS2$_C$*S***	14.6 (9.3)	13.2
^{3}**MECP1$_A$**	2.9 (2.5)	4.1	**PC*R* + *Cat.*$_C$**	−29.5 (−20.6)	−40.6
			PC*S* + *Cat.*$_C$	−29.5 (−20.6)	−40.6
^{1}**RC$_B$**	6.0 (5.3)	7.5	^{oss}**RC$_C$**	1.6 (0.6)	2.2
^{1}**TS1$_B$**	18.3 (17.7)	21.1	^{oss}**TS1$_C$**	21.1 (19.0)	23.5
^{1}**IM$_B$**	4.5 (4.1)	1.6	^{oss}**IM$_C$**	0.1 (−3.1)	−2.2
^{1}**TS2$_B$**	10.3 (6.3)	9.7	^{oss}**TS2$_C$*R***	11.4 (6.0)	10.5
PC + *Cat.*$_B$	−30.0 (−21.2)	−38.8	^{oss}**TS2$_C$*S***	14.6 (9.0)	12.8
^{oss}**RC$_B$**	0.8 (0.3)	1.5	^{3}**RC$_C$**	**0.0 (0.0)**	**0.0**
^{oss}**TS1$_B$**	15.8 (15.1)	17.9	^{3}**TS1$_C$**	21.1 (18.7)	22.5
^{oss}**IM$_B$**	−1.5 (−1.9)	−4.0	^{3}**IM$_C$**	0.2 (−1.0)	−1.0
^{oss}**TS2$_B$**	5.0 (4.8)	7.3	^{3}**TS2$_C$*R***	19.7 (15.2)	21.4
^{3}**RC$_B$**	**0.0 (0.0)**	**0.0**	^{3}**TS2$_C$*S***	20.2 (17.0)	21.0
^{3}**TS1$_B$**	15.3 (15.3)	16.7	^{1}**MECP0$_C$**	7.0 (5.4)	9.4
^{3}**IM$_B$**	−1.1 (−0.8)	−4.0	^{3}**MECP1$_C$**	4.4 (1.4)	4.9
^{3}**TS2$_B$**	15.0 (12.0)	16.9	^{1}**MECP2$_C$*R***	12.4 (7.6)	10.5
^{1}**MECP0$_B$**	6.1 (5.7)	7.6	^{1}**MECP2$_C$*S***	11.8 (6.8)	8.5

dx.doi.org/10.1021/jo402101h | J. Org. Chem. 2013, 78, 12460–12468

the Rh_2–nitrene reactants (^{n}**RC**$_m$), the H-abstraction transition states (^{n}**TS1**$_m$), the intermediates (^{n}**IM**$_m$), the C–N formation transition states (^{n}**TS2**$_m$***l***), and the MECPs (^{n}**MECP0**$_m$, ^{n}**MECP1**$_m$, and ^{n}**MECP2**$_m$***l***), where n = 1 for singlet, OSS for open-shell singlet, and 3 for triplet multiplicities; m = A, B, or C to indicate the reaction involved; and l = *R* or *S* for chiral products in reaction C. The numbers 0, 1, and 2 at the right in these species labels represent the steps of Rh_2–nitrene formation, H-abstraction, and C–N bond formation, respectively. The relative gas-phase free energies, electronic energies, and solvated free energies for all stationary points are shown in Table 1.

(a). Rh_2–Nitrene Character. Calculated bond distances for ^{3}**RC**$_A$ and ^{3}**RC**$_B$ show that the Rh–N and Rh–Rh bonds in triplet ^{3}**RC**$_B$ are longer by 0.076 Å (2.005 Å vs 1.929 Å) and 0.077 Å (2.500 Å vs 2.423 Å) than those in ^{3}**RC**$_A$, respectively (Figure 5). This indicates that the Rh–N bond in ^{3}**RC**$_B$ has a weaker single bond character compared with that in ^{3}**RC**$_A$. Accordingly, there is an increased singlet–triplet free energy gap between ^{3}**RC**$_B$ and ^{1}**RC**$_B$ of 7.5 kcal mol^{-1} (4.5 kcal mol^{-1} between ^{3}**RC**$_A$ and ^{1}**RC**$_A$). The longer Rh–Rh bond of 2.500 Å indicates a weaker metal–metal interaction, so the interaction between the two dirhodiums should be enhanced by the four ligands (Figure 5B), which in turn supports the significant spin density delocalization over the four ligands in ^{3}**RC**$_B$.

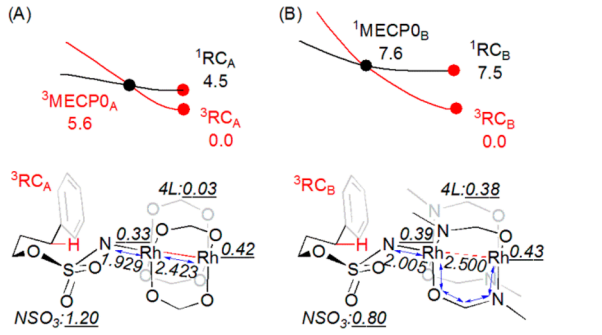

Figure 5. Free energies (kcal mol^{-1}), bond lengths (Å, in italics) and spin densities (in italics and underlined) for the formation of Rh_2–nitrene in reactions A and B. Blue arrows are used to denote the charge and spin transfer course in reactions A and B.

To give a more detailed qualitative description of the Rh_2–nitrene character, we further visualized the Kohn–Sham frontier orbitals (Figure 6). We follow the orbital labeling of our previous analogous Rh_2-based system.[4a] It can be found that the antibonding SOMO1/SOMO2 of ^{3}**RC**$_A$ involves a combination between the N p_y/p_x and Rh–Rh d_{yz}–d_{yz}/d_{xz}–d_{xz} orbitals, and the HOMO–1 orbital has Rh–Rh d_{xy}–d_{xy} character. In reaction B, the antibonding SOMO2 of ^{3}**RC**$_B$ (or ^{OSS}**RC**$_B$) is also between the N p_x and Rh–Rh d_{xz}–d_{xz} orbitals. However, the SOMO1 is antibonding between the N p_x and Rh–Rh d_{xy}–d_{xy} orbitals rather than the N p_y and Rh–Rh d_{yz}–d_{yz} orbitals, which is the HOMO–1 of ^{3}**RC**$_B$ (or ^{OSS}**RC**$_B$). On the basis of the MO coefficients, the SOMO2 of ^{3}**RC**$_A$/^{OSS}**RC**$_B$/^{3}**RC**$_B$ has a larger contribution from the N 2p orbital than SOMO1, where the Rh–Rh d–d orbital is the main component. Therefore, two unpaired electrons reside in the N atom and dirhodium centers, respectively, which intimates that the Rh^{2+}/Rh^{2+} dimer tends to undergo facile one-electron oxidation when combined with related reagents,[2c,h] leading to a mixed-valent Rh^{2+}/Rh^{3+} dimer and a N radical. It should be noted that one of the two unpaired electrons is populated on the Rh–Rh d_{yz}–d_{yz} orbital in ^{3}**RC**$_A$ and the d_{xy}–d_{xy} orbital in ^{OSS}**RC**$_B$/^{3}**RC**$_B$. The acetate and amidate ligands possess p orbitals of appropriate symmetry to combine with the Rh–Rh d_{xy}–d_{xy} orbital rather than the d_{yz}–d_{yz} orbital,[30] showing why the two unpaired electron spins are delocalized significantly (0.38) over the four ligands in ^{3}**RC**$_B$ (or ^{OSS}**RC**$_B$) but only a little (0.03) on the ligand in ^{3}**RC**$_A$. The orbital interactions between the strongly donating *N*-methylformamide groups and dirhodium centers increase the capacity of the dirhodium centers to back-donate to the NSO_3 moiety,[31,2h] so ^{3}**RC**$_B$ (0.80) holds less spin on the NSO_3 moiety than ^{3}**RC**$_A$ (1.20) and acts as a weaker electrophile. Therefore, compared with ^{3}**RC**$_A$, ^{3}**RC**$_B$ can be expected to be less favored for singlet hydride transfer, which intimates a possible mechanism change from the concerted asynchronous nitrene pathway. A metal–nitrene radical generated after metal oxidation has also been recently reported with first-row metal (Fe or Co) complexes.[8a,32]

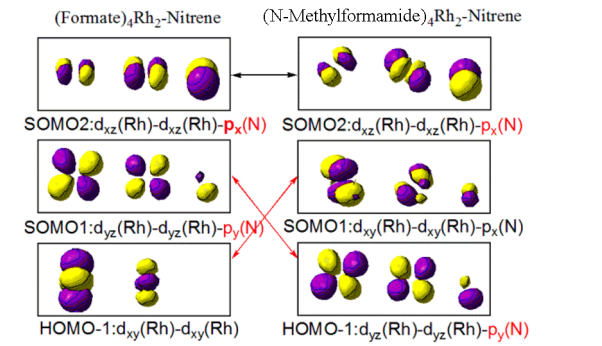

Figure 6. Kohn–Sham frontier orbitals (isovalue: 0.10) of Rh_2–nitrene, HOMO–1, SOMO1, and SOMO2 in reactions A and B.

(b). H Abstraction and C–N Bond Formation in Reaction A. Computed solvation free energy profiles for the C–H insertion of 3-phenylpropylsulfamate ester mediated by Rh_2(formate)$_4$ are shown in Figure 7. The reaction begins with the $Rh_2^{II,III}$–nitrene radical ^{3}**RC**$_A$, which is directly connected to the H-abstraction transition state ^{3}**TS1**$_A$ with an activation free energy of 6.8 kcal mol^{-1}. The triplet transition state ^{3}**TS1**$_A$ is followed by the radical mechanism, where ^{3}**TS1**$_A$ results in a triplet diradical intermediate (^{3}**IM**$_A$) with spin density of 1.00 for the R moiety and 0.43 for the NSO_3 moiety (Figure 1S in the Supporting Information) and a C–N formation transition state ^{3}**TS2**$_A$ with an activation free energy of 5.1 kcal mol^{-1}. However, the existence of ^{3}**MECP1**$_A$ (4.1 kcal mol^{-1}) on the

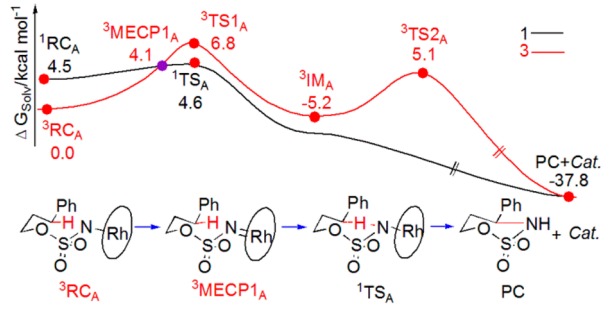

Figure 7. Solvation Gibbs free energy profiles of reaction A at the BPW91/BSII level.

dx.doi.org/10.1021/jo402101h | J. Org. Chem. 2013, 78, 12460–12468

way from ^{3}**RC1**$_A$ to ^{3}**TS1**$_A$ suggests a spin crossover to the closed-shell singlet energy profile. The closed-shell singlet transition state, ^{1}**TS1**$_A$, has a relative free energy of 4.6 kcal mol^{-1}. We searched for the open-shell singlet electronic transition state, but it collapsed to the closed-shell singlet. On the basis of our DFT calculations, the C−H insertion occurs through a direct C−H bond insertion from the Rh$_2^{II,III}$−nitrene radical, where the favored transition state for the reaction is ^{1}**TS1**$_A$, which directly leads to the final product with a large exothermicity (37.8 kcal mol^{-1}).

During the course of the reaction ^{3}**RC**$_A$ → ^{3}**MECP1**$_A$ → ^{1}**TS1**$_A$, the N−H distance is shortened (2.953 Å → 2.445 Å → 1.391 Å), the Rh^1−Rh^2 bond is slightly elongated (2.423 Å → 2.434 Å → 2.435 Å), and the Rh−N bond is reduced by 0.010 Å initially and then increased by 0.062 Å (1.929 Å → 1.919 Å → 1.981 Å) (Figure 8). The Rh−N bond in ^{3}**MECP1**$_A$ thus

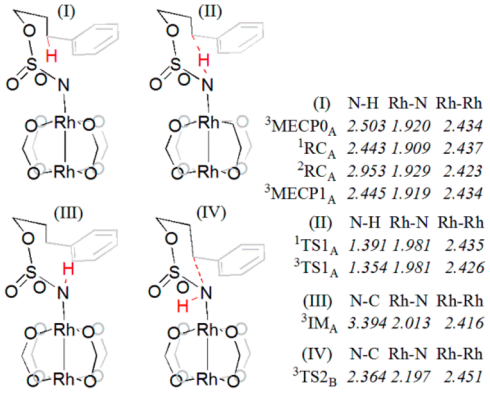

Figure 8. BPW91//BSI structures of stationary points in reaction A. The numbers in italics refer to bond lengths in Å.

holds some double-bond character, and this change is matched with a reduced metal−metal interaction and an elongated Rh^1−Rh^2 bond length.[33] This is also supported by the similarities between ^{3}**MECP1**$_A$ and ^{1}**RC**$_A$ in energy and structure (Figure 8). A resonance form of the metal−ligand bond can be drawn with cationic charge on the N atom center (Figure 9). This

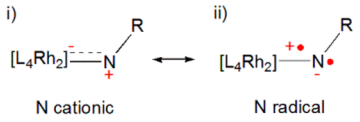

Figure 9. Resonance structures of the Rh$_2$−nitrene: (i) N cationic; (ii) N radical.

cationic character, which is promoted in ^{3}**MECP1**$_A$, enhances the favorability of hydride transfer. The motion of the imaginary vibrational frequency in ^{1}**TS**$_A$ has only hydride transfer character, and the formation of the C−N bond is not visually observed (C−H−N bond angle = 165°).[22] The IRC calculation (Figure 2S in the Supporting Information) also clearly shows that the hydride transfer/C−N bond formation process is a highly asynchronous concerted reaction. Thus, the C−N bond formation is a facile, barrier-free process.

(c). H Abstraction and C−N Bond Formation in Reaction B. Figure 10 shows the computed solvation free energy profile for the analogous Rh$_2$(*N*-methylformamide)$_4$-promoted system. The mechanism for reaction B is qualitatively different from that of reaction A. Starting from the Rh$_2^{II,III}$−

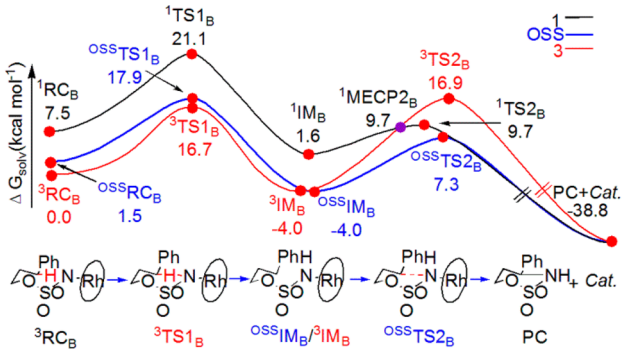

Figure 10. Solvation Gibbs free energy profiles of reaction B at the BPW91/BSII level.

nitrene radical ^{3}**RC**$_B$, the reaction takes place via a triplet H-abstraction transition state (^{3}**TS1**$_B$) with a free energy of activation of 16.7 kcal mol^{-1} relative to ^{3}**RC**$_B$, which is much higher than that of reaction A (^{3}**TS1**$_A$, 6.8 kcal mol^{-1}). In this case, we were able to locate the open-shell singlet transition state (^{OSS}**TS1**$_B$), which is 1.2 kcal mol^{-1} above ^{3}**TS1**$_B$, while the closed-shell singlet transition state (^{1}**TS1**$_B$) is 3.2 kcal mol^{-1} higher in free energy than ^{OSS}**TS1**$_B$. The open-shell singlet profile is generally low enough in free energy to become a more viable mechanism than the closed-shell singlet profile in reaction B. The triplet energy profile then reaches the radical intermediate (^{3}**IM**$_B$), which is −4.0 kcal mol^{-1} below ^{3}**RC**$_B$. The open-shell singlet form of the radical intermediate (^{OSS}**IM**$_B$) has an energy identical to that of ^{3}**IM**$_B$ relative to the reference ^{3}**RC**$_B$ energy (−4.0 kcal mol^{-1}). However, a low-free-energy MECP between the triplet and open-shell singlet energy profiles is not present until the potential curve on the way from ^{3}**RC**$_B$ to ^{3}**TS1**$_B$ (Table 1).[34]

Once these intermediates (^{OSS}**IM**$_B$ and ^{3}**IM**$_B$) are formed, they constitute the starting points for the C−N formation transition states. This step, beginning with the open-shell singlet intermediate ^{OSS}**IM**$_B$, occurs through an open-shell singlet C−N bond formation transition state (^{OSS}**TS2**$_B$) with a relative activation free energy of 7.3 kcal mol^{-1}. The closed-shell singlet transition state (^{1}**TS2**$_B$) is 2.2 kcal mol^{-1} above ^{OSS}**TS2**$_B$, while ^{3}**TS2**$_B$ is a further 7.2 kcal mol^{-1} higher in free energy. The open-shell singlet pathway replaces the triplet as the favored energy profile. Because of the presence of ^{1}**MECP2**$_B$ (9.7 kcal mol^{-1}), the reaction may go through the intersystem crossing (ISC) process from ^{3}**IM**$_B$ to ^{1}**TS2**$_B$. The high-energy ^{3}**TS2**$_B$ transition state plays no role in this reaction. Finally, ^{OSS}**TS2**$_B$ leads to the product complex with a large exothermicity (38.8 kcal mol^{-1}).

It should be noted that the changes in the charge distribution during the reaction are nearly the same for the OSS and triplet states of reaction B (see Figure 3S in the Supporting Information). Qualitative differences mainly appear when examining the spin population (Figure 11). This spin transfer process is qualitatively described in Figure 12. From ^{3}**IM**$_B$ to ^{3}**TS2**$_B$, the spin distributed on the R moiety drops significantly (1.00 → 0.43), which allows inflow to the Rh^1 (0.20 → 0.57) and Rh^2 (0.42 → 0.64) centers. The spin density on the NSO$_3$ and 4L moieties changes little. That is because three electrons localized on the inserted C atom and nitrene N atom in ^{3}**IM**$_B$ cannot form the C−N bond effectively (Figure 12), and one electron occupies an MO with Rh−Rh σ^* bond character in ^{3}**TS2**$_B$. These changes are matched with an increased metal−

dx.doi.org/10.1021/jo402101h | J. Org. Chem. 2013, 78, 12460−12468

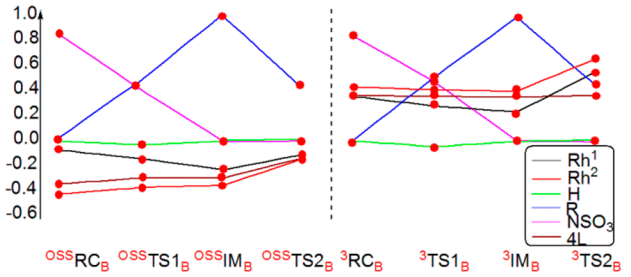

Figure 11. Mulliken spin distribution along the reaction coordinate for the open-shell singlet and triplet states in reaction B.

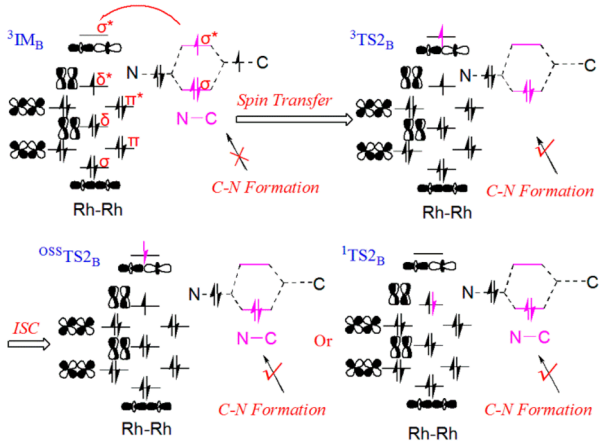

Figure 12. Important molecular orbital interactions involved in the spin transfer and intersystem crossing (ISC) during the C−N bond formation process.

metal interaction and a contracted Rh−Rh bond length of 2.515 Å (^{3}**TS2**$_B$) → 2.473 Å (^{OSS}**TS2**$_B$) → 2.466 Å (^{1}**TS2**$_B$) (Figure 13). Moreover the presence of the heavy Rh atom with

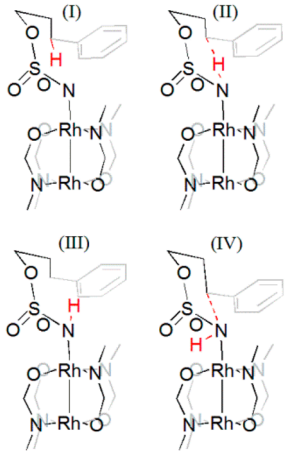

	N-H	Rh-N	Rh-Rh
(I)			
^{1}MECP0$_B$	*4.213*	*1.894*	*2.459*
^{1}RC$_B$	*4.164*	*1.945*	*2.482*
^{2}RC$_B$	*4.050*	*2.007*	*2.500*
^{3}RC$_B$	*4.006*	*2.005*	*2.500*
^{3}MECP1$_B$	*2.476*	*1.997*	*2.502*
(II)	N-H	Rh-N	Rh-Rh
^{1}TS1$_B$	*1.333*	*2.043*	*2.481*
^{2}TS1$_B$	*1.339*	*2.090*	*2.495*
^{3}TS1$_B$	*1.333*	*2.101*	*2.500*
(III)	N-C	Rh-N	Rh-Rh
^{1}IM$_B$	*4.572*	*2.151*	*2.480*
^{2}IM$_B$	*4.629*	*2.137*	*2.481*
^{3}IM$_B$	*4.722*	*2.129*	*2.482*
(IV)	N-C	Rh-N	Rh-Rh
^{1}MECP2$_B$	*2.883*	*2.164*	*2.477*
^{1}TS2$_B$	*2.698*	*2.190*	*2.466*
^{2}TS2$_B$	*2.464*	*2.227*	*2.473*
^{3}TS2$_B$	*2.231*	*2.441*	*2.515*

Figure 13. BPW91//BSI structures of stationary points in reaction B. The numbers in italics refer to bond lengths in Å.

localized parallel spins could enhance the spin−orbit coupling,[15a] thus accelerating the ISC process from the triplet state to the closed- or open-shell singlet state by several orders of magnitude. The existence of MECPs between the closed/open-shell singlet and triplet profiles is required for a state crossing, and then the Rh atom can enhance the ISC.

(d) Mechanism and Enantioselectivity of Reaction C.

To test the validity of the above mechanistic study utilizing model reaction systems, we further investigated the mechanism and enantioselectivity of the synthetically characterized reaction of 3-phenylpropylsulfamate ester catalyzed by Rh_2(*S*-nap)$_4$. The relevant experiments revealed that reaction C tends to occur at the γ-position of the C−H bond, affording homologous six-membered ring products[2h,35] in a chair conformation, and that the phenyl group lies on the equatorial bond. To the best of our knowledge, there is still no X-ray crystal structure for Rh_2(*S*-nap)$_4$. We built the structure of Rh_2(*S*-nap)$_4$ on the basis of the X-ray crystal structure of the complex with the **dzala1** ligand,[36] another dirhodium complex that is very similar to Rh_2(*S*-nap)$_4$. The calculated optimum structure of Rh_2(*S*-nap)$_4$ is shown in Figure 14. The Rh_2(*S*-nap)$_4$ complex belongs to the C_2 point

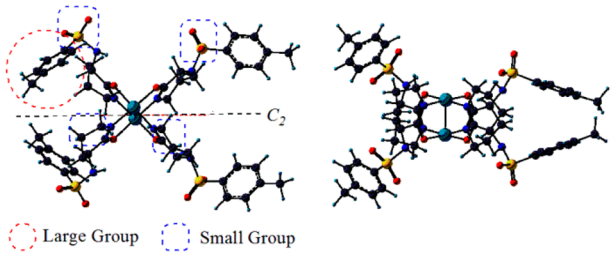

Figure 14. BPW91/BSI structure of Rh_2(*S*-nap)$_4$.

group, so the two rhodium atoms are equivalent to work as a nitrene binding site throughout the reaction. Five moieties, especially one of the sulfonamide moieties (the "Large Group" in Figure 14), lie above the plane defined by Rh and the ligand N and O atoms. Such a conformation requires that the bulky phenyl group of the 3-phenylpropylsulfamate ester approaches the Rh plane opposite this sulfonamide moiety and along the C_2 symmetry axis. We expect that once this orientation is obtained, C−H insertion is rapid. This hypothesis is supported by the calculated enantioselectivity of 3-phenylpropylsulfamate ester catalyzed by Rh_2(*S*-nap)$_4$.

Figure 15 shows the computed solvation free energy profile for the Rh_2(*S*-nap)$_4$-promoted system. In a very similar way to reaction B, the reaction starts from the mixed-valent $Rh_2^{II,III}$−nitrene radical ^{3}**RC**$_C$, and the formation of the radical intermediate ^{3}**IM**$_C$ (−1.0 kcal mol^{-1} below ^{3}**RC**$_C$) has an activation free energy of 22.5 kcal mol^{-1} (^{3}**TS1**$_C$). The open-shell singlet is also an alternative to the triplet since ^{OSS}**TS1**$_C$ is 1.0 kcal mol^{-1} above ^{3}**TS1**$_C$. The closed-shell singlet transition state (^{1}**TS1**$_C$) is a further 2.5 kcal mol^{-1} higher in free energy. The reaction toward the intermediate proceeds through ^{3}**MECP1**$_C$ between the triplet and open-shell singlet profiles (6.7 kcal mol^{-1} above ^{3}**RC**$_C$). The open-shell singlet species (^{OSS}**IM**$_C$) becomes more stable by 1.2 kcal mol^{-1} than the triplet ^{3}**IM**$_C$, so the spin crossover from the triplet state to the open-shell singlet state occurs. The closed-shell singlet ^{1}**IM**$_C$ is 2.5 kcal mol^{-1} higher in energy than ^{3}**IM**$_C$. There is a significant structural difference between Rh_2(*N*-methylformamide)$_4$ and Rh_2(*S*-nap)$_4$. The former is an achiral catalyst, while the latter is a chiral one. Once the intermediate ^{OSS}**IM**$_C$ is formed, a new competition between enantiomers (toward the chiral products) should be considered. The reaction toward the *R* or *S* enantiomer of the product goes through the open-shell singlet transition state ^{OSS}**TS2**$_C$***R*** with an activation free energy of 10.5 kcal mol^{-1} or ^{OSS}**TS2**$_C$***S*** with an activation free energy of 12.8

dx.doi.org/10.1021/jo402101h | J. Org. Chem. 2013, 78, 12460−12468

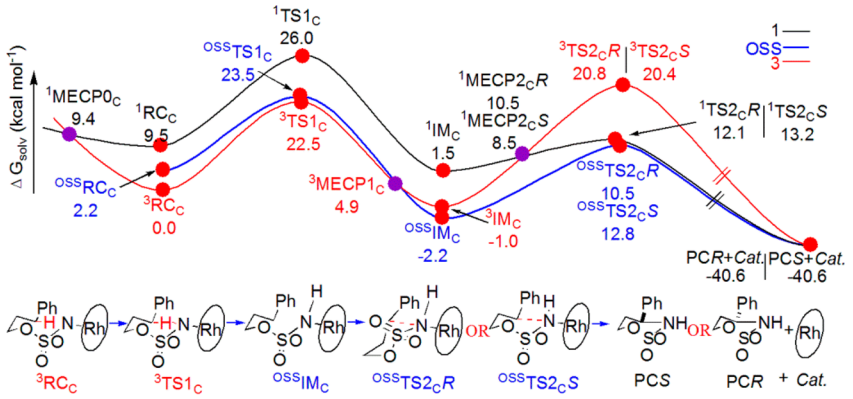

Figure 15. Solvation Gibbs free energy profile of reaction C at the BPW91/BSII level.

kcal mol^{-1}, respectively. The conformations of these two transition states are oriented in such a way that the bulky phenyl group of the 3-phenylpropylsulfamate approaches the Rh plane opposite the sulfonamide moiety and along the C_2 symmetry axis (Figure 16). The substrate lies "above" the Rh

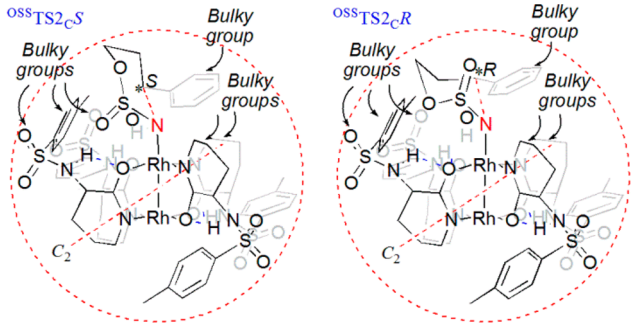

Figure 16. Structural analysis of the two transition states ^{OSS}**TS2$_C$***R* and ^{OSS}**TS2$_C$***S*.

plane defined by Rh and the ligand N and O atoms in **TS2$_C$***R*, which is somewhat similar to that for the Ru-promoted reaction proposed by Blakey and co-workers.[37] The conformation of ^{OSS}**TS2$_C$***S* is similar to those in the diruthenium-promoted reaction proposed by Du Bois[7a] and the Rh-mediated reaction proposed by Liu et al.,[15] with the substrate "standing" on the Rh plane. Therefore, the conformations of ^{OSS}**TS2$_C$***R* and ^{OSS}**TS2$_C$***S* adopted in the present paper show that the substrate avoids a direct approach to the five moieties in Rh$_2$(*S*-nap)$_4$ and can be predicted to be the most stable C–N formation transition states toward the *R* and *S* enantiomers of the product, respectively. The reaction also can proceed through an MECP (^{1}**MECP2$_C$***R* or ^{1}**MECP2$_C$***S*) and subsequent spin crossover from the triplet to the closed-shell singlet profile followed by a closed-shell singlet C–N bond formation transition state (^{1}**TS2$_C$***R* or ^{1}**TS2$_C$***S*). The closed-shell singlet TSs ^{1}**TS2$_C$***R* and ^{1}**TS2$_C$***S* are 1.6 and 0.4 kcal mol^{-1} higher in free energy than ^{OSS}**TS2$_C$***R* and ^{OSS}**TS2$_C$***S*, respectively. The enantioselectivity is mainly determined by the open-shell singlet ^{OSS}**TS2$_C$***R* and ^{OSS}**TS2$_C$***S* species. The calculated enantiomeric excess (Figure 4S in the Supporting Information) is 94.2% and the absolute configuration of the enantiomer was determined to be *R*, in excellent agreement with the experimental results (92% *ee*).[35]

SUMMARY AND CONCLUSION

On the basis of our theoretical computations, we have developed a mechanistic proposal for the intramolecular C–H aminations (Figure 17). The reactions of 3-phenyl-

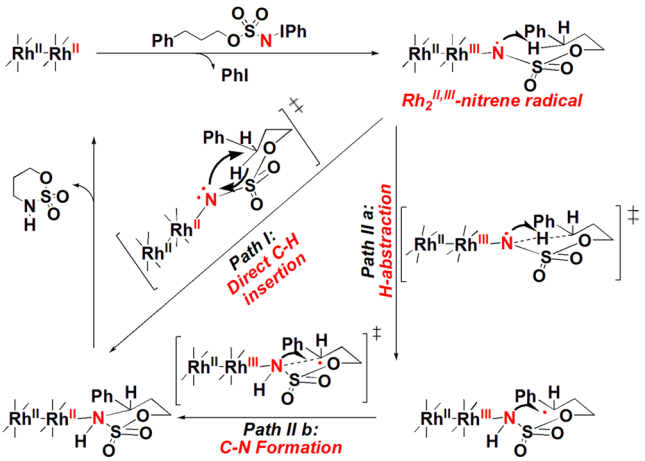

Figure 17. Catalytic cycle proposed for the Rh$_2$(OAc)$_4$- and Rh$_2$(*S*-nap)$_4$-catalyzed reactions of 3-phenylpropylsulfamate.

propylsulfamate catalyzed by the $Rh_2^{II,II}$ complexes start from the oxidation of the $Rh_2^{II,II}$ dimer to a triplet mixed-valent $Rh_2^{II,III}$–nitrene radical, which places radical character on both the dirhodium centers and the nitrene N atom and should facilitate radical H-atom abstraction. However, in the Rh$_2$(formate)$_4$-promoted reaction A, the existence of minimum energy crossing point (MECP) along the process from the $Rh_2^{II,III}$–nitrene radical to the radical H-abstraction transition state leads to a spin crossover to the closed-shell singlet profile. A direct C–H bond insertion then occurs via a highly asynchronous concerted transition state. The analogous Rh$_2$(*N*-methylformamide)$_4$-promoted system (as a model of dirhodium tetracarboxamidate complexes) exhibits a qualitatively different mechanism because of its strongly donating *N*-methylformamide groups. These increase the capacity of the dirhodium centers for back-bonding to the nitrene N atom. Reaction B takes place via a two-step process involving (i) intramolecular H abstraction to generate a diradical intermediate by the triplet pathway, while the open-shell singlet is the alternative to the triplet and the closed-shell singlet can be ignored; and (ii) radical recombination to form the final product with the intersystem crossing (ISC) process from the

dx.doi.org/10.1021/jo402101h | J. Org. Chem. 2013, 78, 12460–12468

triplet to the open-shell singlet state. The mechanism established with the Rh_2(*N*-methylformamide)$_4$ model complex was found to hold in the more complicated reaction of 3-phenylpropylsulfamate esters catalyzed by Rh_2(*S*-nap)$_4$. Therefore, it could be concluded that the mechanism of the Rh_2(*S*-nap)$_4$-catalyzed C−H amination reactions is mainly dependent on the electronic effect of the ligands. Furthermore, the diradical intermediate constitutes the starting point for competition steps involving enantioselectivity, which is determined by the C−N bond formation open-shell singlet transition state. The closed-shell singlet pathway has little effect on the enantioselectivity. The calculated enantiomeric excess was 94.2% with the absolute stereochemistry of the product as *R*, in excellent agreement with the experimental results (92.0% *ee*). The theoretical results presented here will contribute to the rational design of useful synthetic transformations. Further theoretical studies of chemoselective intramolecular C−H insertion reactions are in progress.

■ ASSOCIATED CONTENT

Supporting Information

Cartesian coordinates (in Å); calculated total spin density distributions of selected open-shell stationary points (Table 1S); electronic energies, enthalpies, free energies, and solvation free energies (in hartrees) for all of the relevant species (Table 2S); Mulliken spin distribution along the reaction coordinate for the triplet pathway in reaction A (Figure 1S); IRC from ^1TS_A to the final product (Figure 2S); Mulliken charge distributions along the reaction coordinate for the open-shell singlet and triplet pathways in reaction B (Figure 3S); and a Maxwell−Boltzmann distribution to illustrate the enantioselectivity of C−H amination (Figure 5S). This material is available free of charge via the Internet at http://pubs.acs.org.

■ AUTHOR INFORMATION

Corresponding Authors

*E-mail: ceszhcy@mail.sysu.edu.cn.

*E-mail: cesscy@mail.sysu.edu.cn.

Notes

The authors declare no competing financial interest.

■ ACKNOWLEDGMENTS

C.Z. gratefully acknowledges the National Natural Science Foundation of China (NSFC Projects 20973204, 21173273, and 21373277). Z.K. acknowledges NNSFC funding (21203256). C.-Y.S. acknowledges the 973 Program of China (2012CB821701). This research was conducted using the HKU Computer Centre research computing facilities, which are supported in part by the Hong Kong UGC Special Equipment Grant (SEG HKU09) and the high-performance grid computing platform of Sun Yat-sen University. Computational time was also supported in part by the Guangdong Province Key Laboratory of Computational Science and the Guangdong Province Computational Science Innovative Research Team. We are grateful to Professor Justin Du Bois for providing the X-ray structure of **dzala1**. We thank the reviewers for many insightful comments and suggestions.

■ REFERENCES

(1) (a) Roizen, J. L.; Harvey, M. E.; Du Bois, J. *Acc. Chem. Res.* **2012**, *45*, 911−922. (b) Collet, F.; Dodd, R. H.; Dauban, P. *Chem. Commun.* **2009**, 5061−5074. (c) Davies, H. M. L.; Manning, J. R. *Nature* **2008**, *451*, 417−424. (d) Davies, H. M. L.; Long, M. S. *Angew. Chem., Int. Ed.* **2005**, *44*, 3518−3520. (e) Müller, P.; Fruit, C. *Chem. Rev.* **2003**, *103*, 2905−2920. (f) Yamaguchi, J.; Yamaguchi, A. D.; Itami, K. *Angew. Chem., Int. Ed.* **2012**, *51*, 8960−9009. (g) Hansen, J.; Davies, H. M. L. *Coord. Chem. Rev.* **2008**, *252*, 545−555.

(2) (a) Espino, C. G.; Fiori, K. W.; Kim, M.; Du Bois, J. *J. Am. Chem. Soc.* **2004**, *126*, 15378−15379. (b) Espino, C. G.; Wehn, P. M.; Chow, J.; Du Bois, J. *J. Am. Chem. Soc.* **2001**, *123*, 6935−6936. (c) Fiori, K. W.; Du Bois, J. *J. Am. Chem. Soc.* **2007**, *129*, 562−568. (d) Fleming, J. J.; Du Bois, J. *J. Am. Chem. Soc.* **2006**, *128*, 3926−3927. (e) Guthikonda, K.; Du Bois, J. *J. Am. Chem. Soc.* **2002**, *124*, 13672−13673. (f) Hinman, A.; Du Bois, J. *J. Am. Chem. Soc.* **2003**, *125*, 11510−11511. (g) Wehn, P. M.; Du Bois, J. *J. Am. Chem. Soc.* **2002**, *124*, 12950−12951. (h) Zalatan, D. N.; Du Bois, J. *J. Am. Chem. Soc.* **2008**, *130*, 9220−9221. (i) Zalatan, D. N.; Du Bois, J. *J. Am. Chem. Soc.* **2009**, *131*, 7558−7559. (j) Olson, D. E.; Du Bois, J. *J. Am. Chem. Soc.* **2008**, *130*, 11248−11249. (k) Espino, C. G.; Du Bois, J. *Angew. Chem., Int. Ed.* **2001**, *40*, 598−600.

(3) (a) Kim, J.; Kim, J.; Chang, S. *Chem.—Eur. J.* **2013**, *19*, 7328−7333. (b) Liu, Y.; Che, C.-M. *Chem.—Eur. J.* **2010**, *16*, 10494−10501. (c) Badiei, Y. M.; Dinescu, A.; Dai, X.; Palomino, R. M.; Heinemann, F. W.; Cundari, T. R.; Warren, T. H. *Angew. Chem., Int. Ed.* **2008**, *47*, 9961−9964. (d) Chang, J. W. W.; Chan, P. W. H. *Angew. Chem., Int. Ed.* **2008**, *47*, 1138−1140. (e) Lu, H.; Jiang, H.; Wojtas, L.; Zhang, X. P. *Angew. Chem., Int. Ed.* **2010**, *49*, 10192−10196.

(4) (a) Lin, X.; Zhao, C.; Che, C.-M.; Ke, Z.; Phillips, D. L. *Chem.—Asian J.* **2007**, *2*, 1101−1108. (b) Fiori, K. W.; Espino, C. G.; Brodsky, B. H.; Du Bois, J. *Tetrahedron* **2009**, *65*, 3042−3051. (c) Barman, D. N.; Liu, P.; Houk, K. N.; Nicholas, K. M. *Organometallics* **2010**, *29*, 3404−3412.

(5) (a) Lin, X.; Xi, Y.; Sun, J. *Comput. Theor. Chem.* **2012**, *999*, 74−82. (b) Lin, X.; Sun, J.; Xi, Y.; Pang, B. *Comput. Theor. Chem.* **2011**, *963*, 284−289.

(6) Guo, Z.; Guan, X.; Huang, J.-S.; Tsui, W.-M.; Lin, Z.; Che, C.-M. *Chem.—Eur. J.* **2013**, *19*, 11320−11331.

(7) (a) Harvey, M. E.; Musaev, D. G.; Du Bois, J. *J. Am. Chem. Soc.* **2011**, *133*, 17207−17216. (b) Aguila, M. J. B.; Badiei, Y. M.; Warren, T. H. *J. Am. Chem. Soc.* **2013**, *135*, 9399−9406.

(8) (a) Lyaskovskyy, V.; Suarez, A. I. O.; Lu, H.; Jiang, H.; Zhang, X. P.; de Bruin, B. *J. Am. Chem. Soc.* **2011**, *133*, 12264−12273. (b) Liu, Y.; Guan, X.; Wong, E. L.-M.; Liu, P.; Huang, J.-S.; Che, C.-M. *J. Am. Chem. Soc.* **2013**, *135*, 7194−7204.

(9) (a) Tekarli, S. M.; Williams, T. G.; Cundari, T. R. *J. Chem. Theory Comput.* **2009**, *5*, 2959−2966. (b) Cundari, T. R.; Dinescu, A.; Kazi, A. B. *Inorg. Chem.* **2008**, *47*, 10067−10072.

(10) Fiori, K. W.; Fleming, J. J.; Du Bois, J. *Angew. Chem., Int. Ed.* **2004**, *43*, 4349−4352.

(11) Du Bois, J. *Chemtracts: Org. Chem.* **2005**, *18*, 1−13.

(12) Collet, F.; Lescot, C.; Liang, C.; Dauban, P. *Dalton Trans.* **2010**, *39*, 10401−10413.

(13) Nguyen, Q.; Sun, K.; Driver, T. G. *J. Am. Chem. Soc.* **2012**, *134*, 7262−7265.

(14) Maestre, L.; Sameera, W. M. C.; Díaz-Requejo, M. M.; Maseras, F.; Pérez, P. J. *J. Am. Chem. Soc.* **2013**, *135*, 1338−1348.

(15) (a) Lorpitthaya, R.; Xie, Z.-Z.; Sophy, K. B.; Kuo, J.-L.; Liu, X.-W. *Chem.—Eur. J.* **2010**, *16*, 588−594. (b) Lorpitthaya, R.; Xie, Z.-Z.; Kuo, J.-L.; Liu, X.-W. *Chem.—Eur. J.* **2008**, *14*, 1561−1570.

(16) Mueller, P.; Baud, C.; Naegeli, I. *J. Phys. Org. Chem.* **1998**, *11*, 597−601.

(17) Frisch, M. J.; Trucks, G. W.; Schlegel, H. B.; Scuseria, G. E.; Robb, M. A.; Cheeseman, J. R.; Scalmani, G.; Barone, V.; Mennucci, B.; Petersson, G. A.; Nakatsuji, H.; Caricato, M.; Li, X.; Hratchian, H. P.; Izmaylov, A. F.; Bloino, J.; Zheng, G.; Sonnenberg, J. L.; Hada, M.; Ehara, M.; Toyota, K.; Fukuda, R.; Hasegawa, J.; Ishida, M.; Nakajima, T.; Honda, Y.; Kitao, O.; Nakai, H.; Vreven, T.; Montgomery, J. A., Jr.; Peralta, J. E.; Ogliaro, F.; Bearpark, M.; Heyd, J. J.; Brothers, E.; Kudin, K. N.; Staroverov, V. N.; Kobayashi, R.; Normand, J.; Raghavachari, K.; Rendell, A.; Burant, J. C.; Iyengar, S. S.; Tomasi, J.; Cossi, M.; Rega, N.; Millam, J. M.; Klene, M.; Knox, J. E.; Cross, J. B.; Bakken, V.;

Adamo, C.; Jaramillo, J.; Gomperts, R.; Stratmann, R. E.; Yazyev, O.; Austin, A. J.; Cammi, R.; Pomelli, C.; Ochterski, J. W.; Martin, R. L.; Morokuma, K.; Zakrzewski, V. G.; Voth, G. A.; Salvador, P.; Dannenberg, J. J.; Dapprich, S.; Daniels, A. D.; Farkas, Ö.; Foresman, J. B.; Ortiz, J. V.; Cioslowski, J.; Fox, D. J. *Gaussian 09*, revision A.01; Gaussian, Inc.: Wallingford, CT, 2009.

(18) (a) Becke, A. D. *Phys. Rev. A* **1988**, *38*, 3098−3100. (b) Perdew, J. P.; Burke, K.; Wang, Y. *Phys. Rev. B* **1996**, *54*, 16533−16539.

(19) Harvey, J. N.; Aschi, M.; Schwarz, H.; Koch, W. *Theor. Chem. Acc.* **1998**, *99*, 95−99.

(20) (a) Steinbrenner, U.; Bergner, A.; Dolg, M.; Stoll, H. *Mol. Phys.* **1994**, *82*, 3−11. (b) Henglein, A. *J. Phys. Chem.* **1993**, *97*, 5457−5471. (c) Kaupp, M.; Schleyer, P. v. R.; Stoll, H.; Preuss, H. *J. Chem. Phys.* **1991**, *94*, 1360−1366.

(21) Lam, W. H.; Lam, K. C.; Lin, Z.; Shimada, S.; Perutz, R. N.; Marder, T. B. *Dalton Trans.* **2004**, 1556−1562.

(22) Hansen, J.; Autschbach, J.; Davies, H. M. L. *J. Org. Chem.* **2009**, *74*, 6555−6563.

(23) (a) Feller, D. *J. Comput. Chem.* **1996**, *17*, 1571−1586. (b) Schuchardt, K. L.; Didier, B. T.; Elsethagen, T.; Sun, L.; Gurumoorthi, V.; Chase, J.; Li, J.; Windus, T. L. *J. Chem. Inf. Model.* **2007**, *47*, 1045−1052.

(24) (a) Seeger, R.; Pople, J. A. *J. Chem. Phys.* **1977**, *66*, 3045−3050. (b) Bauernschmitt, R.; Ahlrichs, R. *J. Chem. Phys.* **1996**, *104*, 9047−9052.

(25) Foresman, J. B.; Keith, T. A.; Wiberg, K. B.; Snoonian, J.; Frisch, M. J. *J. Phys. Chem.* **1996**, *100*, 16098−16104.

(26) Marenich, A. V.; Cramer, C. J.; Truhlar, D. G. *J. Phys. Chem. B* **2009**, *113*, 6378−6396.

(27) Ho, J.; Klamt, A.; Coote, M. L. *J. Phys. Chem. A* **2010**, *114*, 13442−13444.

(28) (a) Noodleman, L.; Lovell, T.; Han, W.-G.; Li, J.; Himo, F. *Chem. Rev.* **2004**, *104*, 459−508. (b) Noodleman, L. *J. Chem. Phys.* **1981**, *74*, 5737−5743. (c) Noodleman, L.; Case, D. A. *Adv. Inorg. Chem.* **1992**, *38*, 423−470.

(29) (a) Chan, K. S.; Li, X. Z.; Dzik, W. I.; de Bruin, B. *J. Am. Chem. Soc.* **2008**, *130*, 2051−2061. (b) Knijnenburg, Q.; Hetterscheid, D.; Kooistra, T. M.; Budzelaar, P. H. M. *Eur. J. Inorg. Chem.* **2004**, 1204−1211 and references cited therein.

(30) Lloret, J.; Carbó, J. J.; Bo, C.; Lledós, A.; Pérez-Prieto, J. *Organometallics* **2008**, *27*, 2873−2876.

(31) (a) Padwa, A.; Austin, D. J.; Price, A. T.; Semones, M. A.; Doyle, M. P.; Protopopova, M. N.; Winchester, W. R.; Tran, A. *J. Am. Chem. Soc.* **1993**, *115*, 8669−8680. (b) Pirrung, M. C.; Morehead, A. T. *J. Am. Chem. Soc.* **1994**, *116*, 8991−9000.

(32) (a) Hennessy, E. T.; Betley, T. A. *Science* **2013**, *340*, 591−595. (b) King, E. R.; Hennessy, E. T.; Betley, T. A. *J. Am. Chem. Soc.* **2011**, *133*, 4917−4923. (c) Olivos Suarez, A. I.; Jiang, H.; Zhang, X. P.; de Bruin, B. *Dalton Trans.* **2011**, *40*, 5697−5705.

(33) Nakamura, E.; Yoshikai, N.; Yamanaka, M. *J. Am. Chem. Soc.* **2002**, *124*, 7181−7192.

(34) Through the solvation Gibbs free energy, the open-shell singlet H-abstraction transition state (HATS) has higher energy than the triplet HATS, so the MECP should be located on the way from the HATS to the intermediate. However, the convergence standard in Gaussian software is based on the electronic energy but not the Gibbs free energy. Moreover, the open-shell singlet HATS becomes slightly more stable in electronic energy than the triplet HATS. Therefore, the MECP is located on the way from the Rh_2−nitrene to the HATS. A similar phenomenon has also been observed in previous studies. For example, see: (a) Yu, H. Z.; Fu, Y. *Chem.—Eur. J.* **2012**, *18*, 16765−16773. (b) Gao, H.; Ke, Z.; DeYonker, N. J.; Wang, J.; Xu, H.; Mao, Z.-W.; Phillips, D. L.; Zhao, C. *J. Am. Chem. Soc.* **2011**, *133*, 2904−2915. (c) Shamov, G. A. *J. Am. Chem. Soc.* **2011**, *133*, 4316−4329. (d) Yu, H.-Z.; Jiang, Y.-Y.; Fu, Y.; Liu, L. *J. Am. Chem. Soc.* **2010**, *132*, 18078−18091.

(35) Kang, S.; Lee, H.-K. *J. Org. Chem.* **2010**, *75*, 237−240.

(36) Zalatan, D. N. Ph.D. Thesis, Stanford University, Stanford, CA, 2009.

(37) Milczek, E.; Boudet, N.; Blakey, S. *Angew. Chem., Int. Ed.* **2008**, *47*, 6825−6828.